Synchrotron SAXS Study of Crystallization and Microphase Separation in Compatible Mixtures of Tetrahydrofuran−Methyl Methacrylate Diblock Copolymer and Poly(tetrahydrofuran)

Li-Zhi Liu, Fengji Yeh, and Benjamin Chu*

Department of Chemistry, State University of New York at Stony Brook, Stony Brook, Long Island, New York 11794-3400

Received January 30, 1996; Revised Manuscript Received April 22, 1996[⊗]

ABSTRACT: The crystallization and microphase separation of compatible mixtures of tetrahydrofuran−methyl methacrylate diblock copolymers (PTHF-*b*-PMMA) with a tetrahydrofuran homopolymer (PTHF) were studied by means of synchrotron small-angle X-ray scattering (SAXS) and differential scanning calorimetry (DSC). The crystallization of PTHF microphases in the blend consisting of a PTHF-*b*-PMMA diblock copolymer and a PTHF homopolymer showed almost no effect on the original phase-separated structures in the amorphous state of the blend before crystallization including, for example, the PMMA interdomain distance. In the blends with PMMA lamellar or cylindrical microdomains, the crystallization temperature on cooling and the crystallinity as well as the melting point on subsequent heating of the PTHF microphase were very sensitive to the PTHF lamellar thickness or the distance between the surfaces of two neighboring PMMA cylinders. After crystallization, the blends with an alternating lamellar structure showed an appreciable intensity increase in the higher order scattering peaks, suggesting that the lamellar packing had become more regular. The separation distance between two PMMA cylinders (or spheres) had a great effect on the crystalline structure of the PTHF matrix microphase. When the separation distance between two PMMA cylinders was about 2 times larger than the long period of the neat PTHF homopolymer, a nearly ordered microcrystal packing could be formed in the PTHF matrix microphase. In the blends with 30 wt % or less copolymer and with larger separation distances, the microcrystals could have a very ordered packing, exhibiting sharp X-ray peaks similar to that of the PTHF semicrystalline homopolymer. The PTHF matrix microphase also showed an increase in the long period with increasing copolymer weight fraction. However, this increase in the long period did not result directly from PMMA microdomains. The relationship between the long period and the crystallization temperature was different for blends with different amounts of copolymer.

Introduction

In a compatible blend of an AB diblock copolymer and its corresponding homopolymer A, spherical, cylindrical, lamellar, hexagonally perforated (catenoid) lamellar, bicontinuous *Ia3d* cubic (gyroid), and bicontinuous *Pn-3m* cubic (double diamond) microphases[1−5] can be formed, depending on the blend composition, the copolymer composition, and the temperature. The phase behavior in such AB/A amorphous blends has been studied extensively both experimentally[1−4] and theoretically.[5−7] It could be expected that in AB/A compatible blends with one of the two blocks crystallizable, the crystallization behavior, the structure, and the morphology could be very different from the extensively studied miscible semicrystalline/amorphous homopolymer blends. There have been a few experimental reports[8−10] and a theoretical study[11] on crystallizable AB/A compatible blends. Unlike amorphous AB/A blends, crystallizable AB/A blends actually can be further divided into four different types in terms of whether the amorphous block is "hard", i.e., whether the glass transition temperature, T_g, of the amorphous block is higher than the melting point, T_m, of the crystallizable block, or "soft", i.e., whether T_g is lower than T_m and whether the homopolymer used is amorphous or crystallizable. The crystallization behavior of these four types of AB/A blends could be very different. However, their crystallization behavior may depend on their microphase structure before crystallization, for example, a crystallizable microphase matrix with dispersed amorphous cylinders or spheres.

MacKnight[8] *et al.* studied the crystallization kinetics of mixtures of a symmetric poly(ethylene-*b*-atactic propylene) diblock copolymer with atactic polypropylenes by using the differential scanning calorimetry (DSC) technique. Nojima[9] *et al.* studied the morphology in binary blends of an ϵ-caprolactone−butadiene diblock copolymer (PCL-*b*-PB) with poly(ϵ-caprolactone) by using the SAXS technique. Both copolymers had a "soft" amorphous block. Therefore, the crystallization of their blends was under the influence of soft rubber microphases. The "hard" amorphous microdomains in blends of a semicrystalline−hard amorphous diblock copolymer and its corresponding semicrystalline homopolymer are supposed to have a more significant effect on the crystallization behavior and its final crystalline morphology. A preliminary study[10] on compatible mixtures of a (semicrystalline) tetrahydrofuran-*b*-methyl methacrylate block copolymer (PTHF-*b*-PMMA) with (semicrystalline) PTHF homopolymers showed that, unlike the incompatible AB/A blends of the same polymer composition but with a higher homopolymer molecular weight which rendered the blends incompatible, some unusual crystalline morphologies were observed. The DSC results also showed that the crystallization behavior of incompatible PTHF-*b*-PMMA/PTHF blends was very different, with the compatible blends having just one melting peak and the incompatible blends having two melting peaks. The higher melting peak could be attributed to the melting of the homopolymer-rich macrophase, while the lower melting peak could be attributed to the melting of the PTHF microphase in the copolymer-rich macrophase.

The above studies showed that, in crystallizable AB/A compatible blends, the crystallization behavior and the

* Author to whom correspondence should be addressed.
[⊗] Abstract published in *Advance ACS Abstracts,* June 15, 1996.

Table 1. Characterization of PTHF-*b*-PMMA Diblock Copolymers and PTHF Homopolymers

sample[a]	M_n[b]	W[c](PTHF)	M_n(PTHF block)
TM-1	23300	0.30	7000
TM-2	14000	0.50	7000
PTHF-1	7000		
PTHF-2	2000		

[a] T and M denote abbreviations PTHF and PMMA, respectively. [b] M_n = number-average molecular weight. The listed values have 1−2 significant figures. [c] W = weight fraction.

formation of crystalline morphology could be very complicated and could lead to unusual properties, due to the presence of special structural features. However, all the reported studies were not able to relate the crystallization behavior to each specific microphase morphology in the melt. In the present work, a series of compatible PTHF-*b*-PMMA/PTHF blends with a hard (PMMA) amorphous microphase was used in combination with the synchrotron SAXS and the DSC techniques. First, the microphase morphology of each individual blend in the melt was determined. The microphase-separated and annealed melt was then cooled at different temperatures and the isothermal crystalline structures of the PTHF microphases as well as the microphase morphology and the interdomain structures were investigated after subsequent crystallization from those different initial phase states: (1) alternating amorphous PTHF and hard amorphous PMMA lamellae, (2) amorphous PTHF matrix phase with hexagonally packed hard amorphous PMMA cylinders, and (3) amorphous PTHF matrix phase with dispersed hard amorphous PMMA spheres. Unlike the neat semicrystalline/amorphous diblock copolymers, the thickness of the crystallizable PTHF lamellae and the interdomain distance between the dispersed hard amorphous (PMMA) cylinders or spheres in this AB/A blend can be easily adjusted by solubilizing different amounts of the homopolymer (A ≡ PTHF) within a given concentration range. The microstructures of PTHF-*b*-PMMA/PTHF blends are presented.

Experimental Section

Polymers and Characterization. The synthesis of tetrahydrofuran−methyl methacrylate diblock copolymers (PTHF-*b*-PMMA) and their purification have been described elsewhere.[10] A summary of the pertinent parameters of the PMMA-*b*-PTHF diblock copolymers and the PTHF homopolymers used in the present work is given in Table 1. The composition of the copolymer was determined by proton NMR. The number-average molecular weights (M_n) of the PTHF-*b*-PMMA diblock copolymers and of the PTHF homopolymers were measured by membrane osmometry at 333 K in benzene.

Preparation of Blends. A series of blends of the copolymer TM-1 and low-molecular-weight homopolymer PTHF-2 were prepared by solution casting from chloroform, a nonpreferential solvent for both blocks of the copolymer. A blend of copolymer TM-2 with 10% of PTHF-2 was also prepared by using the same solution-casting procedure. The solvent was evaporated slowly over a period of about 24 h and at room temperature not far from the melting temperature of PTHF so that the microphase morphology could be formed without appreciable effects from the PTHF crystallization. The samples were then examined by SAXS and wide-angle X-ray diffraction (WAXD) to confirm whether the crystallization of PTHF had occurred. To remove the residual solvent and to ascertain the formation of ordered microphase structures, the cast films were placed in a vacuum for 2 days at room temperature and then for 4 h at 373 K. Compositions of the blends, including homopolymer PTHF (homo-PTHF) weight fraction W, M_n(homo-PTHF), W(THF in blend), denoting the total weight fraction of THF in both the block and the homopolymer, and W(H-PTHF in THF phase), denoting the weight fraction of homopolymer PTHF in the THF phase under the assumption of the strong segregation limit (see discussion below), are listed in Table 2 for each of the blends.

Table 2. Compositions of PTHF-*b*-PMMA (TM-1)/PTHF-2 Blends

desig	W(H-PTHF)	M_n(H-PTHF)	W(THF in blend)	W(H-PTHF in THF phase)
TMT1	0.1	2000	0.37	0.27
TMT2	0.2	2000	0.44	0.45
TMT3	0.3	2000	0.51	0.59
TMT4	0.4	2000	0.58	0.69
TMT5	0.5	2000	0.65	0.77
TMT6	0.6	2000	0.72	0.83
TMT7	0.7	2000	0.79	0.89
TMT8	0.8	2000	0.86	0.93
TMT9	0.9	2000	0.93	0.97
PTHF-2	1.0	2000	1.00	1.00

Differential Scanning Calorimetry (DSC). A Perkin-Elmer DSC-2c differential scanning calorimeter was used to study the crystallization of PTHF-*b*-PMMA diblock copolymers and PTHF-*b*-PMMA/PTHF blends. The DSC cooling thermograms were obtained at a rate of −10 K/min from 383 to 213 K, after the samples were annealed for 10 min at 383 K, and then the melting thermograms were obtained at a heating rate of 10 K/min.

Synchrotron Small-Angle X-ray Scattering (SAXS). The scattering experiments were performed at the SUNY X3-A2 beamline of the National Synchrotron Light Source (NSLS), Brookhaven National Laboratory (BNL). The X-ray wavelength used was 0.154 nm. A laser-aided prealigned pinhole collimation system was utilized with a sample to detector distance of 1065 mm.[12] Small angles down to 1.5 mrad with a d-spacing ($d = 2\pi/q_{min}$) of about 100 nm were achieved. Fuji imaging plates were used to collect the scattering data with exposure times of 5 min per frame. A constant-temperature device, which could either cool or heat by means of a Peltier element over a temperature range of 273−343 K, was used to control the sample temperature to ±0.2 K. The blends were first studied in the melt state. The scattering data were collected after each sample was annealed for 10 min at 333 K, above the melting temperature of PTHF. The samples were then quenched to 288 K for 80 h, 283 K for 10 h, and 275 K for 6 h, respectively, to isothermally crystallize PTHF. This set of crystallization conditions ensured the completion of isothermal crystallization for all the samples. The details will be discussed in the next section. The SAXS measurements of the crystallized samples were performed at 283 K.

Results and Discussion

For the AB/A blends listed in Table 2, the compatibility of a diblock copolymer with its corresponding homopolymer is strongly dependent on the molecular weight ratio of the homopolymer to its corresponding block; the smaller the ratio is, the better the compatibility of the blend. The previous study[10] on PTHF-*b*-PMMA/PTHF blends showed that the compatibility could easily be determined from their melting behavior. Two distinct melting peaks were observed for the incompatible blends. All blends used in the present work were compatible. The cast films in the melt state were transparent and showed one macroscopic phase under direct observation in an optical microscope, in agreement with the DSC result showing only one melting peak.

1. Microphase Morphologies of the Blends and Neat Copolymer in the Melt State. The microphase morphology for each individual blend in the melt state (above the melting temperature of PTHF) was determined on the basis of scattering peak positions from SAXS. Figures 1 and 2 show, respectively, SAXS

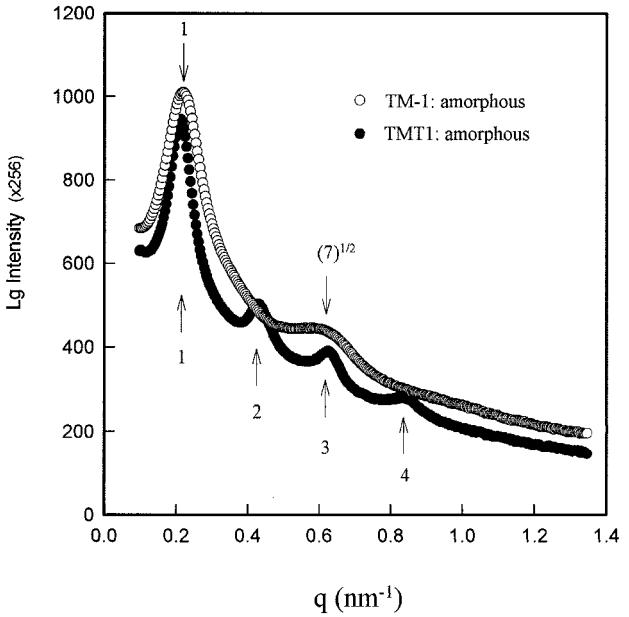

Figure 1. SAXS profiles of copolymer TM-1 and blend TMT1 (see Table 2) with 10% PTHF homopolymer.

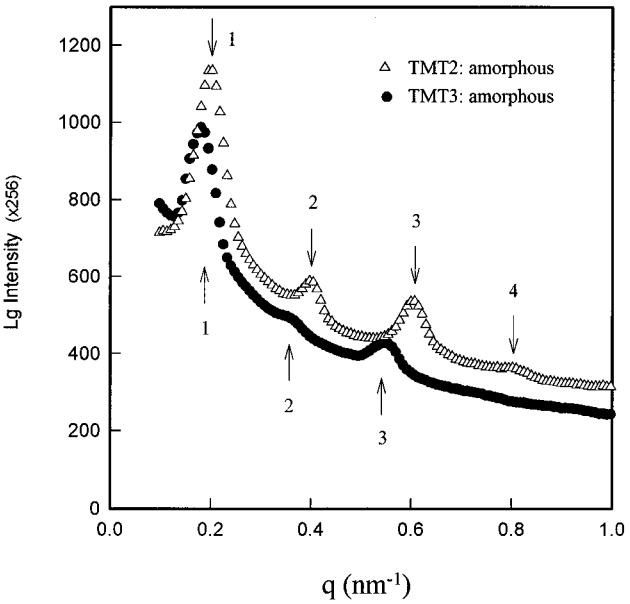

Figure 2. SAXS profiles of blends TMT2 and TMT3 (see Table 2) with 20% and 30% PTHF homopolymer.

profiles of the blends with 10% (TMT1) and 20% (TMT2) PTHF homopolymer, exhibiting multiple-order scattering maxima at peak positions of 1:2:3:4, relative to that of the first-order peak. This peak position ratio implies the existence of an alternating PTHF and PMMA lamellar structure with a long-range order. The sample with hexagonally packed cylindrical microdomains can exhibit scattering maxima with peak position ratios of $1:(3)^{1/2}:(4)^{1/2}:(7)^{1/2}:(9)^{1/2}:(12)^{1/2}:(13)^{1/2}:(16)^{1/2}$. The blends with 40% (TMT4) and 50% (TMT5) PTHF homopolymer show scattering maxima at peak positions of $1:(4)^{1/2}:(9)^{1/2}:(13)^{1/2}$ and of $1:(4)^{1/2}:(7)^{1/2}:(13)^{1/2}$, respectively, with only the TMT5 blend displayed in Figure 3. The higher order peak position ratios implied that hexagonally packed PMMA cylinders were formed in these two blends. The scattering peaks in Figure 3 correspond, respectively, to d_{100}, d_{200}, d_{210}, and d_{310}, where d_{hk0} is the lattice spacing of the (hk0) planes of the hexagonal packing. The blend with 30% homopolymer, as shown in Figure 2, exhibited scattering maxima at peak

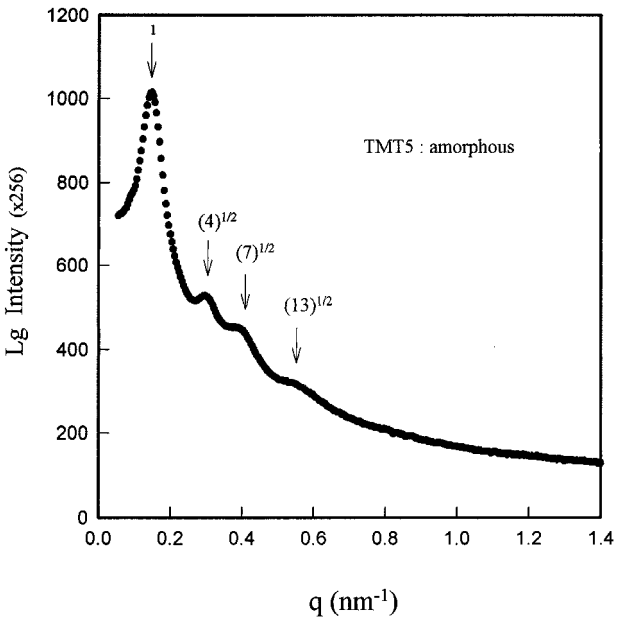

Figure 3. SAXS profile of blend TMT5 (see Table 2) with 50% PTHF homopolymer.

positions of 1:2:3. No peaks were observed at the relative peak positions of $(3)^{1/2}$, $(7)^{1/2}$, and $(12)^{1/2}$, suggesting an alternating lamellar structure for this blend. The neat copolymer TM-1, as shown in Figure 1, exhibited scattering maxima at peak positions of $1:(7)^{1/2}$, suggesting the presence of a PTHF cylindrical microphase. One might suspect that by comparing the two SAXS profiles in Figure 1, the microphase structure for the TM-1 copolymer could be lamellar. However, by adding 10% or 20% PTHF homopolymer to the TM-1 copolymer, the microphase structure of the blend TMT1 was clearly lamellar in nature, as shown in Figures 1 and 2. Furthermore, with TMT3, as shown in Figure 2, the lamellar structure began to deteriorate, and at TMT5, the blend has transformed to a cylindrical morphology with PMMA, instead of PTHF as postulated in Figure 1, forming the cylindrical microphase.

The blends with 60% and 80% PTHF homopolymer exhibited a clear first-order scattering peak and only one additional higher order peak, as shown in Figure 4. The scattering maxima were observed for the blend with even 90% homopolymer. The first peak intensity decreased with increasing homopolymer content. By considering the THF weight fractions of these blends, ranging from 0.72 to 0.93 for TMT6 to TMT9, the dispersed microdomains were likely to be made up of PMMA spheres. Table 3 summarizes the microphase morphology of these blends as shown in Figures 1−4 in the melt (amorphous) state.

The interdomain distance D can be determined from the corresponding Bragg spacings[1]

$$D = d_{001} \tag{1}$$

for the alternating lamellar structure

$$D = (4/3)^{1/2} d_{100} \tag{2}$$

for the hexagonally packed cylindrical microdomains, and

$$D = (3/2)^{1/2} d_{110} \tag{3}$$

for the spherical microdomains with body-centered cubic

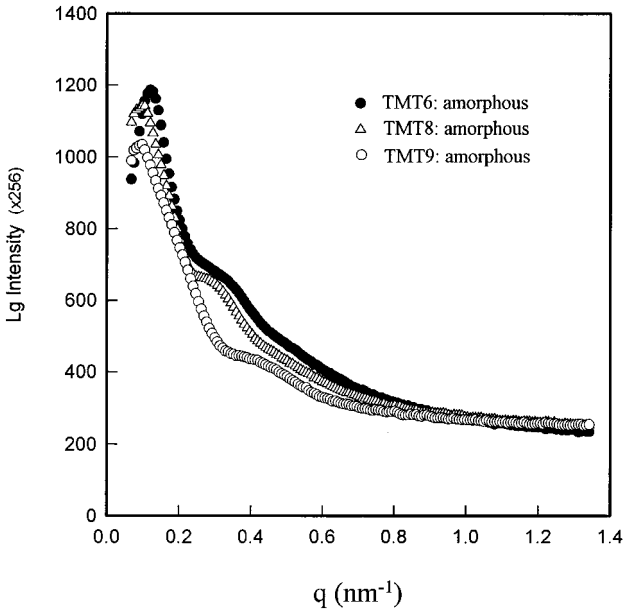

Figure 4. SAXS profiles of the blends TMT6, TMT8, and TMT9 (see Table 2) with 60%, 80%, and 90% PTHF homopolymer.

Table 3. Microphase Morphology of Blends Studied

desig	*W*(THF in blend)[a]	microphase morphology
TM-1 copolymer	0.30	(PTHF cylinder)
TMT1	0.37	lamella
TMT2	0.44	lamella
TMT3	0.51	lamella
TMT4	0.58	PMMA cylinder
TMT5	0.65	PMMA cylinder
TMT6	0.72	(PMMA sphere)
TMT7	0.79	(PMMA sphere)
TMT8	0.86	(PMMA sphere)
TMT9	0.93	(PMMA sphere)

[a] Including PTHF homopolymer and PTHF block of the copolymer.

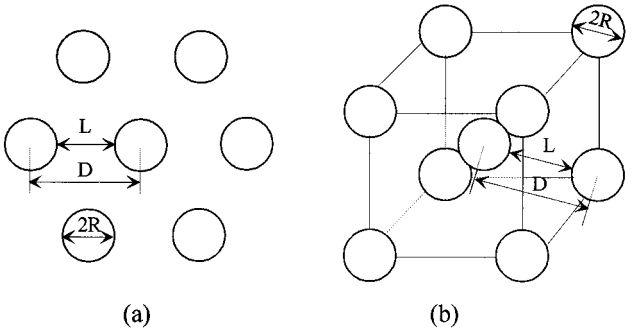

Figure 5. (a) hexagonally close-packed PMMA cylinders and (b) spheres with a body-centered cubic lattice with definitions of *R*, *L* and *D*.

(bcc) symmetry. Figure 5 shows a schematic representation of the interdomain distance *D* (a) having hexagonally packed cylindrical microdomains and (b) for spherical microdomains with bcc symmetry. The separation distance *L* between the surfaces of two neighboring PMMA cylinders (or of the body-center sphere and the corner sphere) is also defined in Figure 5 for future discussions on the crystallization behavior of the blends. The Bragg spacing of the first-order scattering peak ($d = 2\pi/q_{1\text{st-order peak}}$) of the neat copolymer and that of the blends together with their average interdomain distance *D* are shown in Figure 6. The interdomain distance of the blends with spherical microdomains was calculated based on the bcc structure assumption. The above

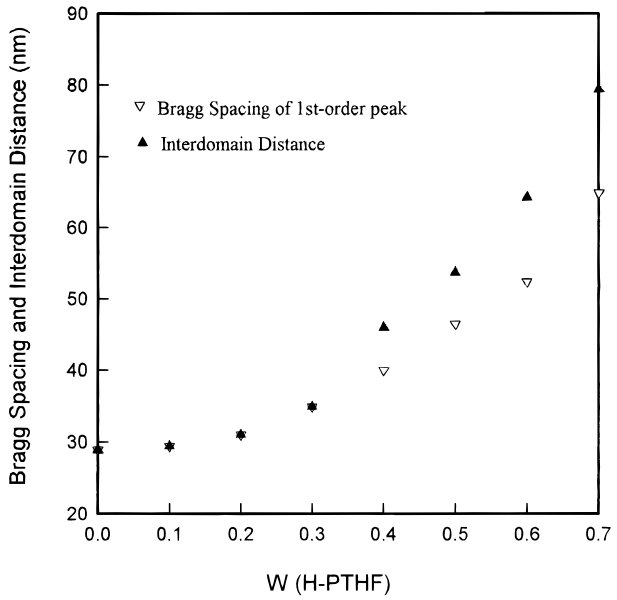

Figure 6. Bragg spacing (*d*) of first-order scattering peak and interdomain distance (*D*) of neat copolymer TM-1 and its blends with 10% up to 70% PTHF homopolymer in the amorphous state. See eqs 1−3 for relations between *D* and d_{hk0}.

Table 4. DSC Results of the Neat Copolymer and Homopolymer

sample	*W*(PTHF)	M_n(PTHF block)	T_c (K)	T_m (K)	X_c (%)
TM-1	0.30	7000		289	18[a]
PTHF-2	1.00	2000	277	296	55

[a] Crystallinity of PTHF block = X_c = heat of the fusion of copolymer/(W(THF)·$\Delta H°_m$).

results about the changes in the microphase morphology and in the interdomain distance with the solubilized homopolymer confirmed the fact that the blends were compatible. The results will be discussed further in section 3 on the isothermal crystalline structure of the THF microphase of the blends.

2. Crystallization Behavior of the Neat Copolymer and Homopolymer. In order to explain the crystallization behavior of the compatible PTHF-*b*-PMMA/PTHF blends, it is also necessary to know the crystalline features of the neat copolymer and of the homopolymer. The suggested dispersed PTHF cylindrical morphology in the neat copolymer, as shown in Figure 1, could cause the PTHF microdomains to have a very weak crystallizability because PTHF in the dispersed phase has restricted dimensions. This supposition on weak crystallizability was confirmed by a DSC nonisothermal crystallization study. Upon cooling from 383 to 213 K and at a cooling rate of 10 K/min, the homopolymer used in this work showed a crystallization peak with a maximum position at $T_c = 277$ K, while no crystallization peak was observed for the neat copolymer by using the same cooling process. The melting point (T_m) and the degree of crystallinity (X_c) of the neat copolymer and of the homopolymer, obtained from the subsequent heating process, together with the crystallization temperature T_c, are listed in Table 4. The enthalpy of fusion of PTHF, $\Delta H°_m = 12.4$ kJ mol^{-1},[13] i.e. $\Delta H°_m = 172.2$ J/g, was used to calculate the degree of crystallinity of the THF phase in the copolymer TM-1. Although no crystallization peak was observed during cooling for the neat copolymer, a melting peak appeared during the subsequent heating process at a rate of 10 K/min. However, the melting point of the neat copolymer at 289 K was 17 deg lower than that of the

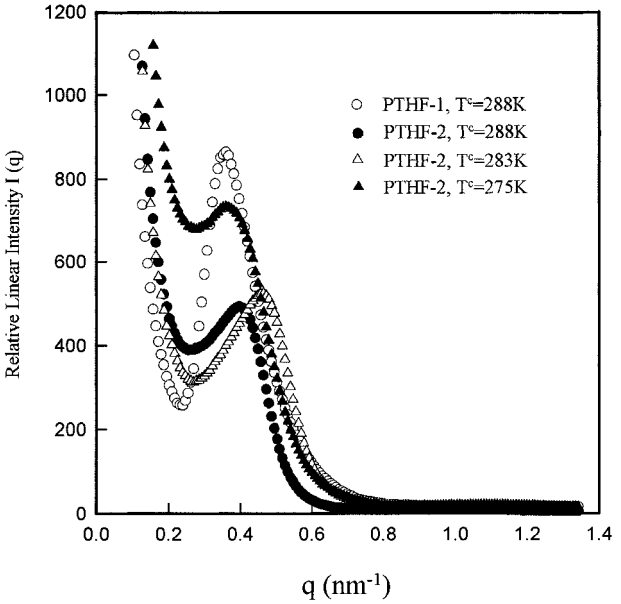

Figure 7. SAXS profiles of the prepolymer PTHF-1 crystallized at 288 K and of the homopolymer PTHF-2 crystallized at 288, 283, and 275 K, respectively.

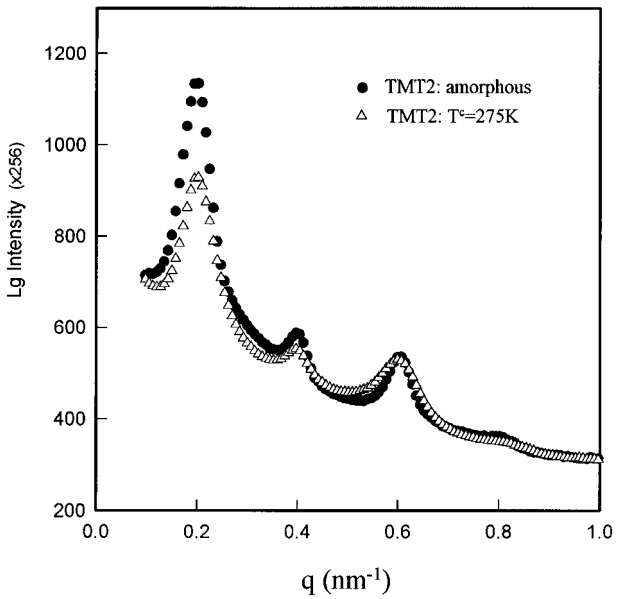

Figure 8. SAXS profiles of TMT2 (see Table 2) in the amorphous state (filled circles) and of TMT2 crystallized at 275 K (hollow triangles).

PTHF homopolymer, mainly due probably to the limited size of the PTHF microcylinders. The crystallinity of the PTHF block in the copolymer with $X_c = 18\%$ was also much lower than that of the PTHF homopolymer with $X_c = 55\%$. The absence of T_c over the practical temperature range down to near T_g of PTHF implies that nucleation and crystallization of the neat copolymer are much slower than those of the PTHF homopolymer due to the restricted dimensions of the dispersed PTHF phase.

The SAXS study of the PTHF homopolymer (PTHF-2) used in the blends and the prepolymer PTHF-1, which is identical with the PTHF block of the copolymer, showed that the prepolymer exhibited a much sharper scattering peak than that of the homopolymer with lower molecular weight, as shown in Figure 7. The sharper peak, denoted by hollow circles in Figure 7, suggests a more regular packing of the lamellar stacks in the prepolymer. Under the same crystalline condition, the prepolymer PTHF-1 has a larger long period than that of the homopolymer PTHF-2, i.e. 17.5 and 15.8 nm, respectively, when crystallizing at 288 K. Although the PTHF prepolymer (PTHF-1) showed a sharp SAXS peak (see Figure 7), the SAXS profiles of the neat copolymer in the melt (denoted by hollow circles in Figure 1) and in the crystallized state showed almost no difference, because the PTHF blocks could only be crystallized in the dispersed microcylinders. In Figure 7, the long period of PTHF-2 first decreased with decreasing temperature from 288 to 283 K and then increased with decreasing temperature from 283 to 275 K. The latter observation could be due to the fact that 275 K was lower than the T_c (see Table 4) of PTHF-2 homopolymer.

3. Isothermal Crystalline Structures of PTHF Microphases of the Blends. When blended with the copolymer, the PTHF homopolymer is solubilized into PTHF microdomains of the copolymer, thereby increasing the nucleation and crystallization ability of the microdomains. The homopolymer molecules in the lamellar microdomains have fewer conformational constraints than the corresponding block. In a recent SANS study,[14] the homopolymer molecules were found to be unperturbed in lamellar microdomains, at least in the direction parallel to the lamellae. The nonisothermal crystallization kinetics study showed that the T_c increased from 262 to 271 K for the blends containing 10−50% homopolymer, indicating that crystallizability became stronger when more homopolymers were solubilized into the microdomains. On the other hand, a large difference in T_c for blends with different compositions implied a corresponding difference in time for the blends to complete their isothermal crystallization at a given temperature. The isothermal crystalline morphology study[15] showed that all the blends with ≥30% homopolymer exhibited visible crystalline morphologies in an optical microscope with polarized light after having crystallized the sample at 288 K for 10 h, while it took only a few minutes for the pure homopolymer to complete the crystallization process at 288 K. In the present work, the following crystallization conditions were set: 288 K for 80 h, 283 K for 10 h, and 275 K for 6 h to ensure completion of crystallization for all the samples. In fact, under these crystallization conditions, even the neat copolymer became turbid when removed from the temperature-controlled water bath.

3.1. Crystallization of PTHF Lamellar Microphase. The blends with 10−30% homopolymer had lamellar structures in the melt. The blends TMT2 and TMT3 were then crystallized at 275 K for 6 h, and their SAXS profiles in Figures 8 and 9 showed the same peak positions as the corresponding peak positions of the blends in the melt state, indicating they still had lamellar structures. The fact that the lamellar structure remained unchanged is reasonable, since the glass transition temperature of PMMA lamellae is much higher than 275 K, and hence it is very difficult to change the morphology by crystallization in the PTHF lamellae. As also shown in Figures 8 and 9, the scattered intensity of the first-order peak decreased appreciably after crystallization. This decrease could be attributed to a decrease in density difference between PMMA (1.190) and PTHF lamellae, whose density is 0.982 in the amorphous phase and 1.144 in the crystallized phase, as estimated from an average of the five reported values[13] for the density in the crystalline phase. As will be presented below, all the blends

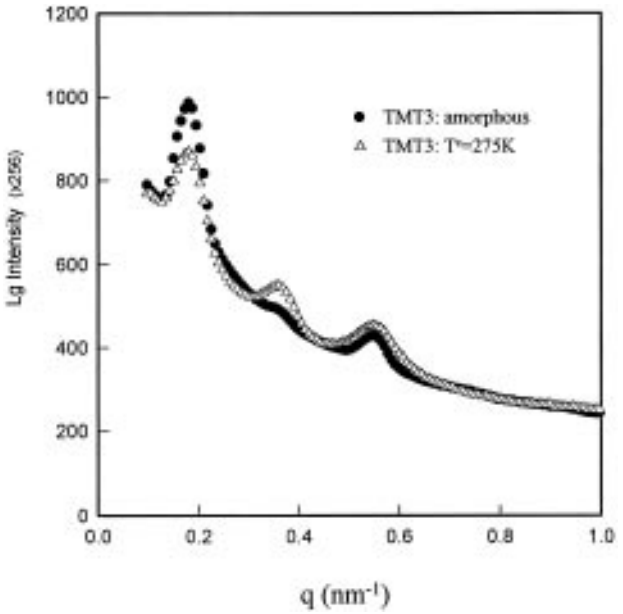

Figure 9. SAXS profiles of TMT3 (see Table 2) in the amorphous state (filled circles) and of TMT3 crystallized at 275 K (hollow triangles).

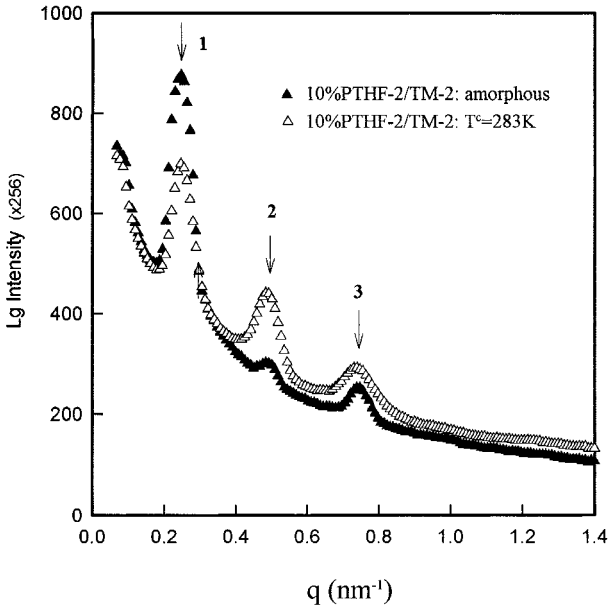

Figure 10. SAXS profiles of amorphous (filled triangles) and crystallized (hollow triangles) blend of copolymer TM-2 with 10% PTHF-2 homopolymer.

showed a large decrease in the intensity of the first-order peak. Therefore, this difference can, in turn, be used as an indication of crystallization in the blends, especially for those crystallized samples, such as TMT1 to TMT3, whose only change in the SAXS profiles was the decrease in scattered intensity of the first-order peak. The decrease in the density difference between the microdomains of PMMA and PTHF could also produce a corresponding intensity decrease in the higher order peaks if the microdomain structures remained the same after crystallization. However, the higher -order peak intensity remained almost the same for the TMT2 blend with 20% homopolymer, as shown in Figure 8, and an obvious increase, instead of a decrease, in the higher order peak intensity was observed for the TMT3 blend with 30% homopolymer, as shown in Figure 9. To provide more evidence about such scattering behavior of the blends with a lamellar structure, an additional blend, consisting of 10% of the same homopolymer PTHF-2 and another copolymer (TM-2) with 50% PTHF content as listed in Table 1, was studied both in the melt state at 333 K and after crystallization of the sample at 283 K. This blend had an alternating lamellar structure, as shown in Figure 10, which revealed a much larger increase in the intensity of its higher order peaks after crystallization. The increase in intensity in the higher order peaks of the above blends (TMT3 in Figure 9 and TM-2/10%PTHF-2 in Figure 10) suggested that after crystallization the lamellar packing became much more regular than that in the melt state. The above results showed that the crystallizability of PTHF in the PTHF lamellae could be increased by solubilizing more PTHF homopolymer in PTHF lamellae or by increasing the PTHF content in the copolymer. The higher the crystallizability, the higher the intensity of higher order peaks after crystallization. Thus, the higher crystallizability resulted in more regular lamellar packing in the blend after crystallization. After crystallization, the PTHF lamellae could become nonuniform as the lamellar layer had to be composed of both crystallized and amorphous PTHF.

In the strong segregation limit, the thicknesses of the PTHF and PMMA layers and the spatial distribution[1]

Table 5. Lamellar Structure Characterization and DSC Results of Blends TMT1 to TMT3

sample	D_{PMMA} (nm)	D_{PTHF} (nm)	a_J/a_{J1}	T_c (K)	T_m (K)	X_c (%)[a]
TMT1	17.2	12.2	1.00	262	293	26
TMT2	15.9	15.1	1.04	264	294	28
TMT3	15.4	19.5	1.06	269	296	34

[a] X_c is the crystallinity of PTHF phase.

of added homopolymer within the PTHF phase can also be estimated from SAXS together with volumetric considerations.[1] The structural parameters and the parameters (T_c, T_m, and X_c in the PTHF lamellar microphase) from DSC, as listed in Table 5, can be used to help us understand the crystallization kinetic behavior. The strong segregation limit means that the PTHF homopolymer is completely solubilized into PTHF microdomains and that the PTHF block of the copolymer and the homopolymer are completely segregated from PMMA. In fact, the degree of incompatibility between PMMA and PTHF is relatively high, so that, even for the PTHF-*b*-PMMA copolymer with as low a molecular weight as $M_n = 8400$, the copolymer is well phase-separated by the presence of a strong first-order peak in the SAXS study. The blend TMT9 with only 7% PMMA still showed a microphase-separated structure in Figure 4. Based on the strong segregation limit, the thickness of PMMA lamellar microdomains can be calculated with the equation[1]

$$D_{PMMA} = \phi_b f D \tag{4}$$

where ϕ_b is the volume fraction of the copolymer in the blend, f is the volume fraction of the PMMA block in the copolymer (i.e. $\phi_b f$ is the volume fraction of PMMA in the blend), and D is the interdomain distance of the blend. The interdomain distance of blends TMT1 to TMT3 and the calculated thicknesses of the PMMA and PTHF lamellae are listed in Table 5. The density of PMMA, 1.190, and the density of amorphous PTHF, 0.982, were used in calculating ϕ_b in eq 4.

The distance a_J between the chemical junctions of the copolymer could be changed with addition of the homo-

polymer[1] and could also be estimated. For alternating lamellar microdomains, we have

$$D/D_0 = (\rho_J/\rho_{J0})\phi_b \quad (5)$$

where D_0 is the interdomain distance of the neat copolymer, D is the interdomain distance of the blend, ρ_J and ρ_{J0} are the interfacial density of the chemical junctions of the block copolymer after and before the homopolymer addition, and ϕ_b is the volume fraction of the copolymer in the blend. From the measured value of D/D_0 and the known value of ϕ_b, one can calculate[1] the expansion a_J/a_{J0}, where a_J and a_{J0} are the average nearest-neighbor distances between the chemical junctions after and before the addition of the homopolymer, and

$$a_J/a_{J0} = (\rho_J/\rho_{J0})^{1/2} \quad (6)$$

With the above two equations, we can calculate, a_{J2}/a_{J1} and a_{J3}/a_{J1}, the expansion of the nearest-neighbor distances of blends TMT2 and TMT3 relative to TMT1, with all three blends forming lamellar microdomains. The calculated values of a_J/a_{J1} are also listed in Table 5.

In Table 5, it can be seen that the average thickness of PMMA lamellae (D_{PMMA}) decreased only slightly with increasing homopolymer weight fraction, resulting in little expansion of the average nearest-neighbor distance a_J of the blends TMT2 and TMT3 relative to that of blend TMT1 (a_{J1}). Therefore, the additional 20% homopolymer in TMT3, when compared with that of TMT1, must have been solubilized mainly toward the middle of the PTHF lamellae. The average thickness of the PTHF lamellae increased from 12.2 to 19.5 nm with addition of 20% more homopolymer into the blends. The crystallization kinetic behavior in these confined PTHF microphases of the blends TMT1 to TMT3 was supposed to be very sensitive to the PTHF lamellar thickness, which was of the order of magnitude of the long period of the PTHF homopolymer (about 17 nm under the same crystalline conditions).

The DSC nonisothermal crystallization kinetic results of the blends are also given in Table 5. The crystallization temperature T_c was obtained on cooling from 383 to 213 K at a rate of 10 K/min, and the melting point T_m and the crystallinity X_c were obtained on subsequent heating at the same rate. The results showed that the crystallization temperature T_c of blend TMT3 was 5 K higher than that of blend TMT2, and 7 K higher than that of blend TMT1, indicating that the crystallizability of the PTHF lamellar microphase became stronger with increasing PTHF lamellar thickness. The crystallinity and the melting point of the PTHF lamellar microphase also showed the same dependence; i.e., the thicker the PTHF lamellar phase, the higher the X_c and T_m became. The T_m of blend TMT3 was 3 K higher than that of blend TMT1 and 7 K higher than that of the neat copolymer TM-1 (see Table 4). By comparing the thickness of the PTHF lamellar microphase in the blends with the long period of PTHF-2 homopolymer (~17 nm), it can be concluded that the blend can have the same melting point as that of PTHF homopolymer (296 K, as listed in Table 4) only when the average thickness of the PTHF lamellar microphase is larger than the long period of the homopolymer. However, the PTHF microphase showing the same T_m as that of the homopolymer could not reach the same crystallinity as the homopolymer. In Tables 4 and 5, the X_c of PTHF microphase in blend TMT3 was only 62% of that of the homopolymer. This decrease in crystallinity could be attributed to the lower crystallinity of the PTHF block located near the interface region.

Table 6. Characterization of Hexagonally Packed PMMA Cylinders in Blends TMT4 and TMT5 and of PMMA Spheres with Assumed bcc Symmetry in Blends TMT6 and TMT7

sample	W(H-PTHF)	W(THF)	D (nm)	R_{PMMA} (nm)	L (nm)
TMT4	0.4	0.58	46.0	14.7	16.6
TMT5	0.5	0.65	53.7	15.7	22.3
TMT6	0.6	0.72	64.2	22.8	18.6
TMT7	0.7	0.79	79.4	25.4	28.6

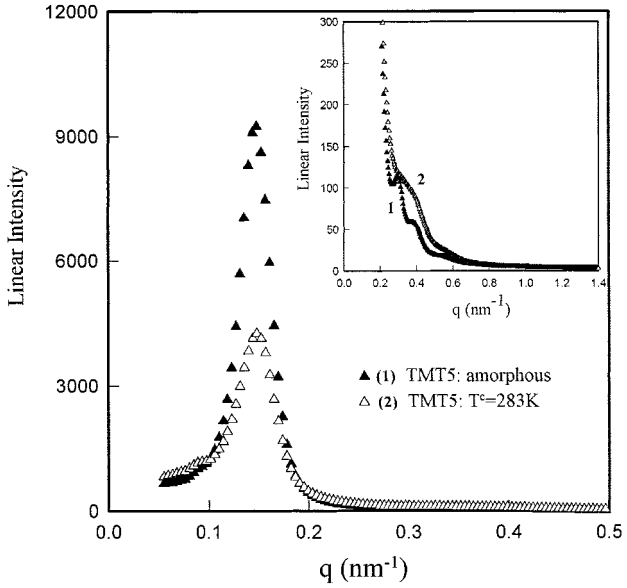

Figure 11. SAXS profiles of amorphous and crystallized blend TMT5 (see Table 2) with 50% PTHF homopolymer.

3.2. Crystallization of PTHF Matrix Microphase with Dispersed PMMA Cylinders. The blends TMT4 and TMT5 with 40% and 50% PTHF homopolymer have hexagonally packed PMMA cylinders as the dispersed microphase. Based on the strong segregation limit, the average radius R_{PMMA} of the hexagonally packed PMMA cylinders can be estimated from volumetric considerations,[1]

$$R_{PMMA} = (3)^{1/4}(f\phi_b/(2\pi))^{1/2}D \quad (7)$$

where D is now the interdomain distance of the PMMA cylinders. The values of D, R_{PMMA}, and L, defined as the average distance between the surfaces of the two PMMA cylinders in Figure 5a, are listed in Table 6 for blends TMT4 and TMT5 in the amorphous state.

The nucleation and crystal growth of PTHF in a matrix microphase in the blend are supposed to be easier than that of PTHF in a more restrictive lamellar phase. However, the scattering maximum from PTHF microcrystals was still more than 40 times smaller than the first-order scattering maximum of microphase separation between PTHF and PMMA. As the scattering maximum from PTHF microcrystals appeared in the q-range comparable with the higher order peaks of microphase separation, SAXS profiles in Figures 11–14 are presented in the linear intensity scale.

The two blends, TMT4 and TMT5 from the amorphous state to the state after the sample had been crystallized at 283 K, showed an appreciable decrease in the intensity of the first-order scattering peak, as

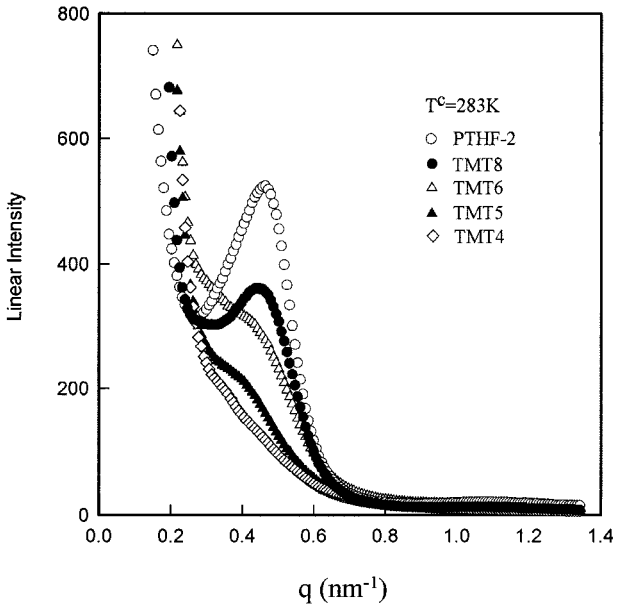

Figure 12. Crystalline scattering profiles of blends with 40% up to 80% PTHF homopolymer and neat homopolymer PTHF-2. Crystallization temperature at 283 K.

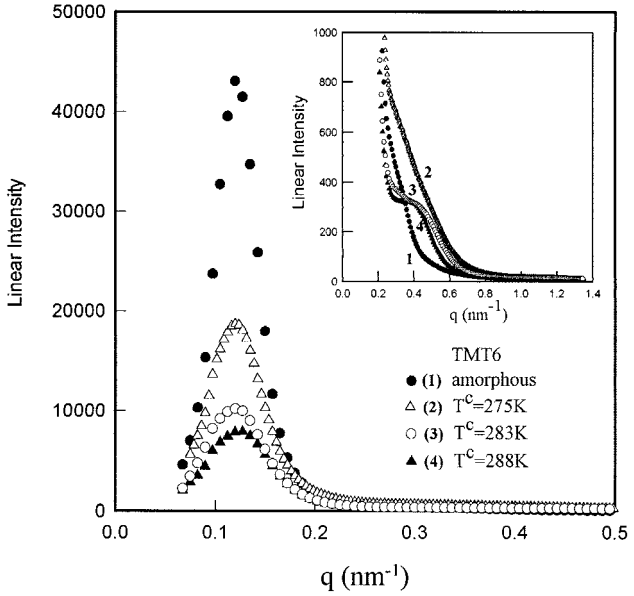

Figure 13. SAXS profiles of blend TMT6 with 60% homopolymer in the amorphous state and crystallized at different temperatures.

shown in Figure 11 for blend TMT5. The decrease in the intensity of the first-order peak after crystallization is due to the decrease in the density difference between PMMA and PTHF microphases. The first-order scattering peak of blends TMT4 and TMT5 remained almost at the same position after crystallization, indicating that after crystallization the microphase-separated structure of PTHF and PMMA had remained the same. The constant interdomain distance implied that the crystallization of PTHF in the PTHF matrix phase did not affect the distribution of the hard PMMA cylinders. However, since the long period of the PTHF homopolymer crystallized at 283 K was 13.5 nm and the separation distance L between the PMMA cylinders was still less than 2 times the long period, the crystallization kinetic behavior and the crystalline structure formation of the PTHF matrix microphase could also be very sensitive to the separation distance L. The nonisothermal DSC study showed that the crystallization temperature (T_c) of blends TMT4 and TMT5 on cooling from 383 K at a rate of 10 K/min was 270 and 271 K, respectively, indicating that with more homopolymer being solubilized into the PTHF microphase, the separation distance L became larger and the crystallizability became stronger. Since the value of L in the PTHF microphase was larger than the long period of the homopolymer, both blends showed the same melting point, 296 K, on subsequent heating at the same rate. However, the crystallinity of TMT5, 44%, was obviously higher than that of TMT4, 39%, due to the higher homo-PTHF weight fraction in the PTHF microphase of TMT5 (see Table 2). The scattering behavior of blends TMT4 and TMT5 at higher q-values could be explained in terms of the difference in the crystalline structures due to different PTHF phase sizes L. The crystalline scattering shoulder of TMT5 near $q = 0.4$ nm^{-1}, as shown in the inset of Figure 11, suggested that ordered microcrystals with a long period of about 16 nm ($\approx 2\pi/q_m$) were formed in the matrix microphase. Blend TMT4 showed little increase in the intensity at higher q-values (not shown), suggesting that microcrystals formed in the matrix microphase were not ordered sufficiently due to the smaller separation distance L.

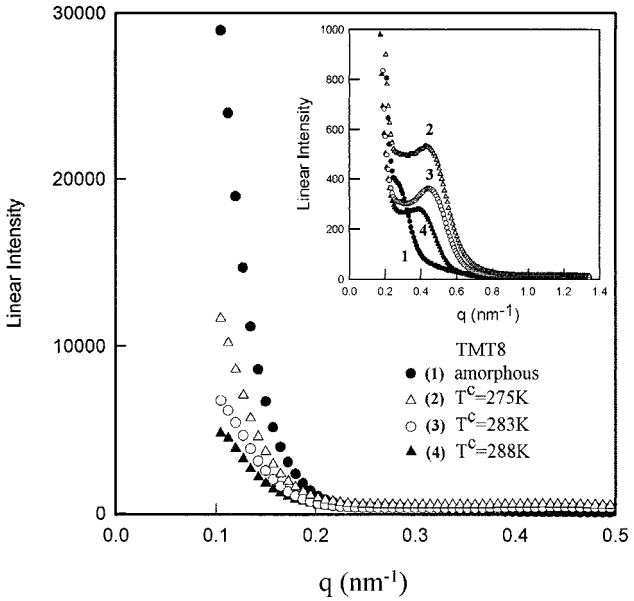

Figure 14. SAXS curves of blend TMT8 with 80% homopolymer in the amorphous state and crystallized at different temperatures.

3.3. Crystallization of PTHF Matrix Microphase with Dispersed PMMA Spheres. The blends with 60−90% PTHF homopolymer were supposed to form dispersed PMMA spherical microdomains considering their THF weight fractions ranging from 0.72 to 0.93, as discussed in the morphology section. It is very helpful to know the average radius and the distance between the surface of two neighboring PMMA spheres. To be able to estimate these parameters, a bcc packing mode is assumed in the discussion. Based on the strong segregation limit, the average radius R_{PMMA} of the spherical microdomains with bcc symmetry can be estimated from volumetric considerations,[1]

$$R_{PMMA} = (3)^{-1/6}(f\phi_b/\pi)^{1/3}D \qquad (8)$$

where D is now the interdomain distance of the PMMA

spheres. The values of D, R_{PMMA}, and L (shown in Figure 5b) are also listed in Table 6 for blends TMT6 and TMT7 in the amorphous state.

A large decrease in the first-order peak intensity was again observed after the sample had been crystallized from the amorphous state. Figure 12 shows the crystalline scattering parts of the SAXS profiles in a linear scale for blends TMT6 and TMT8 and the PTHF-2 homopolymer. SAXS profiles of blends TMT4 and TMT5 are also presented as references. All the samples were crystallized at 283 K for 10 h. The peak position shifted to lower q-values with increasing homo-PTHF fraction in the blends. The corresponding long periods were 13.5 and 14.2 nm for the neat homopolymer and blend TMT8 with 80% homopolymer and about 15 and 16 nm for blends TMT6 and TMT5 containing 60% and 50% homopolymer, respectively. It is noted that the first-order peak position of the microphase separation in these blends did not shift appreciably after crystallization, as shown in Figure 13 for TMT6, and the interdomain distance of these spheres remained almost the same. Thus, unlike miscible amorphous/semicrystalline homopolymer blends, the increase in the long period with increasing copolymer weight fraction could not result from the location of dispersed PMMA component in between the PTHF crystals. In fact, the PMMA cylinder diameter (~30 nm; see Table 6) and the PMMA sphere diameter (~50 nm; see Table 6) were even much larger than the long period (~13 nm; see Figure 12) of the PTHF crystals in the PTHF matrix microphase, and the scattering peak position of microphase separation between PTHF and PMMA (see Figure 13) did not change after crystallization. The increase in the long period and the lowering of T_c and of X_c with increasing copolymer weight fraction presumably resulted from an increase in the packing of condensed PMMA microdomains in the blends. The presence of more PMMA made crystallization slower and yielded crystals with a longer long period. The effect is similar to crystallization at a higher temperature. The crystalline scattering shoulder of blend TMT6 was much higher than that of TMT5, as shown in Figure 12. A clear crystalline scattering peak appeared for TMT8 and TMT7 (not shown). The results illustrate that when the separation distance is large, the crystal packing can be regular. For TMT7, $L \approx 30$ nm, which is about twice the long period, and a fairly sharp peak is observed, while for TMT6, $L \approx 19$ nm, which is only slightly larger than the long period, and only a shoulder is present in Figure 12.

3.4. Structures of Blends TMT6 and TMT8 Crystallized under Different Temperatures. The nucleation and crystal growth of polymers are very sensitive to the isothermal crystallization temperature. In a PTHF matrix microphase with dispersed spherical PMMA microdomains, whose diameter $2R_{PMMA}$ is comparable to or even larger than the separation distance L of the spheres, the temperature-dependent crystallization behavior could be different from the corresponding semicrystalline homopolymers. Blends TMT6 and TMT8 with 28% and 14% PMMA content, respectively, were chosen for such a study. The SAXS curves of these two blends crystallized at 275, 283, and 288 K, respectively, as well as the SAXS profile in the melt, are shown in Figures 13 and 14. The first-order peak corresponds to the microphase separation structure. However, for TMT8 the first-order was not reached due to the limit of the experimental setup at the time of the synchrotron run. Both figures also showed a large decrease in the intensity of the first-order peak after crystallization. These two figures further showed that the higher the crystallization temperature, the larger the decrease in the intensity of the first-order peak. The larger decrease could result from the higher crystallinity of the PTHF phase and hence the smaller density difference between the PMMA microphase and the PTHF microphase. When the PTHF matrix microphase crystallized quickly at a lower temperature, it had a lower crystallinity than the PTHF which had been crystallized slowly at a higher temperature.

When blends TMT6 and TMT8 were crystallized isothermally at different temperatures, the crystalline scattering peak at $q \approx 0.4$ nm^{-1} showed an intensity increase with decreasing crystallization temperature, especially for the TMT8 blend, as shown in Figures 13 and 14. The increase in the scattered intensity with decreasing crystallization temperature was similar to that of the PTHF-2 homopolymer, as shown in Figure 7. However, the long period or peak position dependence on the isothermal crystallization temperature was different between the TMT6 blend and the TMT8 blend, both of which are different from the PTHF-2 homopolymer. The PTHF-2 homopolymer and the TMT8 blend with 80% PTHF-2 homopolymer showed a decrease in the long period with decreasing crystallization temperature from 288 to 283 K. With further decrease in the crystallization temperature from 283 to 275 K, PTHF-2 homopolymer showed an increase in the long period, but the TMT8 blend did not show any further change in the long period, as shown in Figures 7 and 14. The TMT6 blend with less PTHF-2 homopolymer than the TMT8 blend showed little long period dependence on the isothermal crystallization temperature, ranging from 288 K down to 275 K, as shown in Figure 13. The above results indicated that the long period dependence on the isothermal crystallization temperature could be different for blends with different separation distance L, which was 18.6 nm for TMT6 (28.6 nm for TMT7) and was estimated to be more than 30 nm for TMT8. A sharp crystalline scattering peak was observed for TMT8 blend with 14% PMMA whether it was crystallized at 288, 283, or 275 K, as shown in Figure 14. However, only a crystalline scattering shoulder (or a sloping line) was observed for the TMT6 blend with 28% PMMA, as shown in Figure 13, indicating that the PTHF crystal packing became less regular with increasing amount of PMMA content dispersed in the PTHF matrix microphase. With the isothermal crystallization temperature of the TMT6 blend decreasing from 283, to 275 K, the crystalline scattering profile changed from a wide crystalline scattering shoulder (denoted by hollow circles and filled triangles as shown in Figure 13) into a sloping line (denoted by hollow triangles in Figure 13), indicating that the crystal packing of the blend with a larger weight fraction of PMMA microdomains became less regular (sloping line) when it was crystallized at a lower temperature, i.e., at 275 K. The less regular crystal packing in the TMT6 blend when compared with that in the TMT8 blend could essentially be attributed to the decrease in the separation distance L (as defined in Figure 5b) for the TMT6 blend.

Conclusions

1. The PMMA microphases (whether lamellar, cylindrical, or spherical microdomains) remained essentially unchanged when the blend was crystallized from the

melt. Moreover, the crystallization of the PTHF microphase did not show an obvious effect on the interdomain distance (D) of the blends.

2. After crystallization from the melt, all the blends showed an appreciable decrease in the intensity of the first-order scattering peak due to the microphase separation between PTHF and PMMA. The higher the isothermal crystallization temperature, the larger the decrease in the first-order peak intensity. This decrease in the first-order peak intensity could be attributed to a decrease in the density difference between the PMMA and the PTHF microphases after crystallization. The intensity dependence on crystalline temperature suggested that the higher the crystallization temperature, the higher the crystallinity of the PTHF microphase became.

3. With alternating PTHF and PMMA lamellar microdomains, the average thickness (e.g., $D_{PTHF} \approx 15$ nm for TMT2) of PTHF lamellae was comparable to the long period of the PTHF homopolymer (e.g., long period $\approx$ 17 nm for PTHF-2). The crystallization kinetics behavior in this confined PTHF microphase was very sensitive to the PTHF lamellar thickness. In the DSC study, the crystallization temperature from the cooling curve and the crystallinity and the melting point of such a PTHF lamellar microphase on a subsequent heating curve increased with increasing lamellar thickness, indicating that the crystallizability of the PTHF lamellar microphase became higher when the PTHF microphase became thicker by solubilizing more PTHF homopolymers into the PTHF microphase. With the thickness of the PTHF lamellar microphase being larger than the magnitude of the long period of the homopolymer under the same crystallization conditions, the PTHF microphase had the same melting point as that of the PTHF homopolymer. However, the crystallinity of the PTHF microphase was still much smaller than that of the PTHF homopolymer, mainly because of the lower crystallinity of the PTHF block located near the interface region.

4. After crystallization from the melt, the higher order scattering peaks of the blends with an alternating lamellar structure increased, in contrast with the appreciable decrease in the first-order peak which is due to the decrease in the density difference between PMMA and PTHF. The increase in intensity in the higher order peaks of the blends (TMT3 in Figure 9 and TM-2/10%PTHF-2 in Figure 10) suggested that after crystallization the lamellar packing became much more regular than that in the melt state.

5. In the presence of PMMA cylinders with the separation distance L being about twice that of the long period of the neat PTHF homopolymer, a strong crystalline scattering shoulder in the high q-range (e.g., see hollow triangles in the inset of Figure 11) could be detected, suggesting a nearly ordered microcrystal packing in the PTHF matrix microphase. The crystallization temperature T_c and the crystallinity from DSC also showed an increase with increasing separation distance L.

6. In the isothermal crystallization study, the long period of the PTHF microphase increased with increasing copolymer weight fraction, presumably because the presence of PMMA microdomains could slow down the crystallization and tend to make the crystals pack with a longer period, the same tendency as homopolymer crystallization at a higher temperature.

7. The separation distance L between the PMMA microdomains had a great effect on the crystalline structure of the PTHF matrix microphase. The microcrystals could have ordered packing only when the separation distance L was sufficiently large, i.e., more than twice that of the long period of the neat homopolymer in blends TMT7 and TMT8. The long period dependence on the isothermal crystallization temperature could be different for the blends with different separation distance L.

Acknowledgment. B.C. gratefully acknowledges support of this work by the National Science Foundation, Polymers Program (DMR9301294), the Department of Energy (DEFG0286ER 45237), and the U.S. Army Research Office (DAAH0494G0053).

References and Notes

(1) Tanaka, H.; Hasegawa, H.; Hashimoto, T. *Macromolecules* **1991**, *24*, 240.
(2) Winey, K. I.; Thomas, E. L.; Fetters, L. J. *Macromolecules* **1992**, *25*, 2645.
(3) Jeon, K.-J.; Roe, R.-J. *Macromolecules* **1994**, *27*, 2439.
(4) Zhao, J.; Majumdar, B.; Schulz, M. F.; Bates, F. S.; Almdal, K.; Mortensen, K.; Hajduk, D. A.; Gruner, S. M. *Macromolecules* **1996**, *29*, 1204.
(5) Matsen, M. W. *Macromolecules* **1995**, *28*, 5765
(6) Whitmore, M. D.; Noolandi, J. *Macromolecules* **1985**, *18*, 2486.
(7) Olvera de la Cruz, M.; Sanchez, I. *Macromolecules* **1987**, *20*, 440.
(8) Sakurai, K.; MacKnight, W. J.; Lohse, D. J.; Schulz, D. N.; Sissano, J. A. *Macromolecules* **1994**, *27*, 4941.
(9) Nojima, S.; Takahashi, Y.; Ashida, T. *Polymer* **1994**, *35*, 2853.
(10) Liu, L.-Z.; Li, H.; Jiang, B.; Zhou, E. *Polymer* **1994**, *35*, 5511.
(11) Whitmore, M. D.; Noolandi, J. *Macromolecules* **1988**, *21*, 1482.
(12) Chu, B.; Harney, P. J.; Li, Y.; Linliu, K.; Yeh, F.; Hsiao, B. S. *Rev. Sci. Instrum.* **1994**, *65*, 597.
(13) Dreyfuss, P. *Poly(tetrahydrofuran)*; Gordon and Breach: New York, 1982.
(14) Matsushita, Y.; Torikai, N.; Mogi, Y.; Noda, I.; Han, C. C. *Macromolecules* **1994**, *27*, 4566.
(15) Liu, L.-Z. *et al.*, to be published.

MA960143Z